Supporting Information

Layered hydrotalcites derived holey porous cobalt oxide nanosheets coated by nitrogen-doped carbon for high-mass-loading Li-ion storage

Long Pan [a,b,#,*], *Yicheng Wei* [a], *ZhengMing Sun* [a,*], *Markus Niederberger* [b]

[a] *Key Laboratory of Advanced Metallic Materials of Jiangsu Province, School of Materials Science and Engineering, Southeast University, Nanjing, 211189, China*

[b] *Laboratory for Multifunctional Materials, Department of Materials, ETH Zurich, Vladimir-Prelog-Weg 5, 8093, Zurich, Switzerland*

* *Emails: panlong@seu.edu.cn; zmsun@seu.edu.cn*

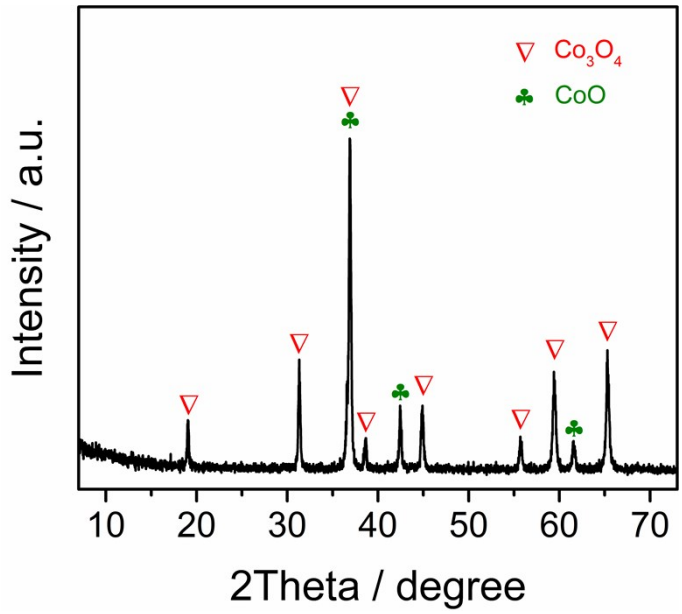

Figure S1. XRD pattern of holey Co_3O_4 nanosheets annealed at 500 ℃ for 2 hours in Ar atmosphere with a ramping rate of 2 ℃ min^{-1}. The main phase is Co_3O_4. Besides, the reflections of CoO emerged, indicating that partial of Co_3O_4 was decomposed into CoO ($2Co_3O_4 \rightarrow 6CoO + O_2\uparrow$) in argon atmosphere.[S1, S2] For Co_3O_4@PDA, however, the Co_3O_4 was completely converted to CoO (Fig. 3a) during the annealing process, implying that the NC induces the reduction of Co_3O_4 because of the high reducibility of carbon ($2Co_3O_4 + C \rightarrow 6CoO + CO_2\uparrow$).[S2]

Note that this pattern was recorded on a DX-2700BH (HaoYuan) X-ray diffractometer equipped with a monochromator, while other XRD patterns were recorded on PANalytical Empyrean X-ray diffractometer without a monochromator.

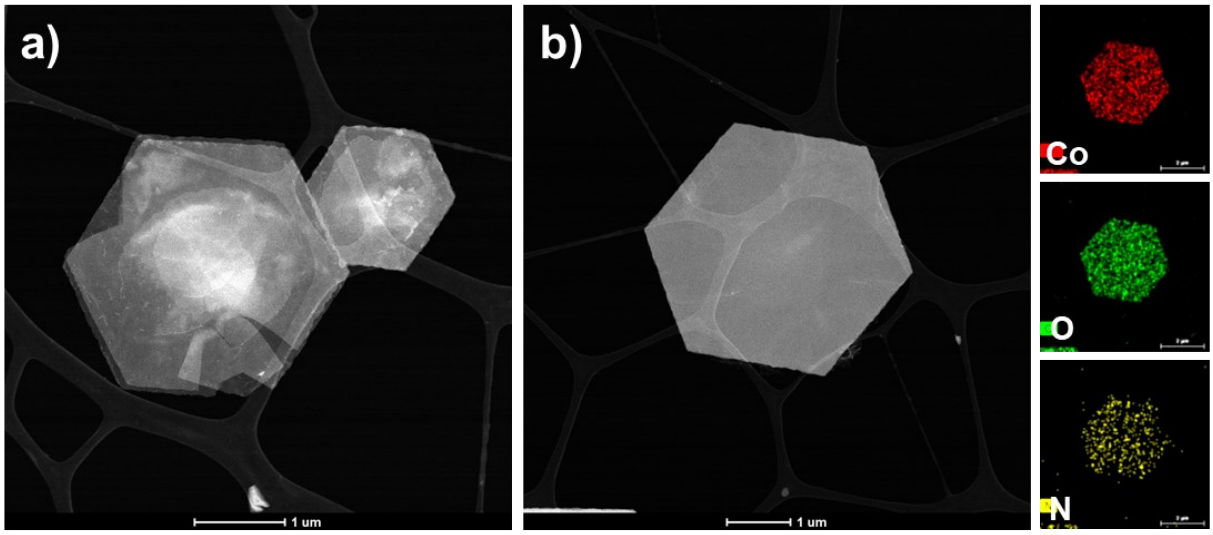

Figure S2. (a) STEM image and (b) STEM image with element mappings of the LCH nanosheets.

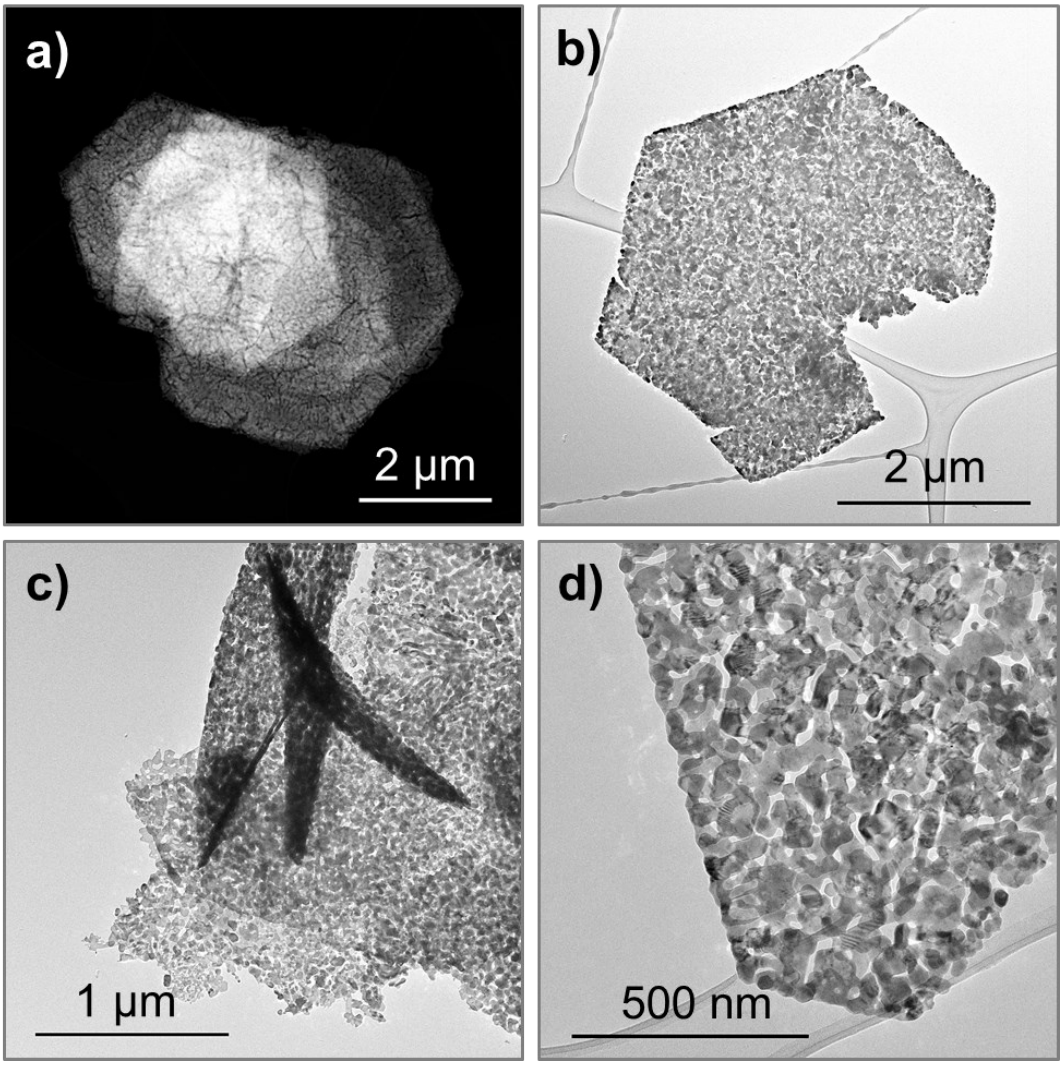

Figure S3. (a) STEM and (b−d) TEM images of the holey Co_3O_4 nanosheets.

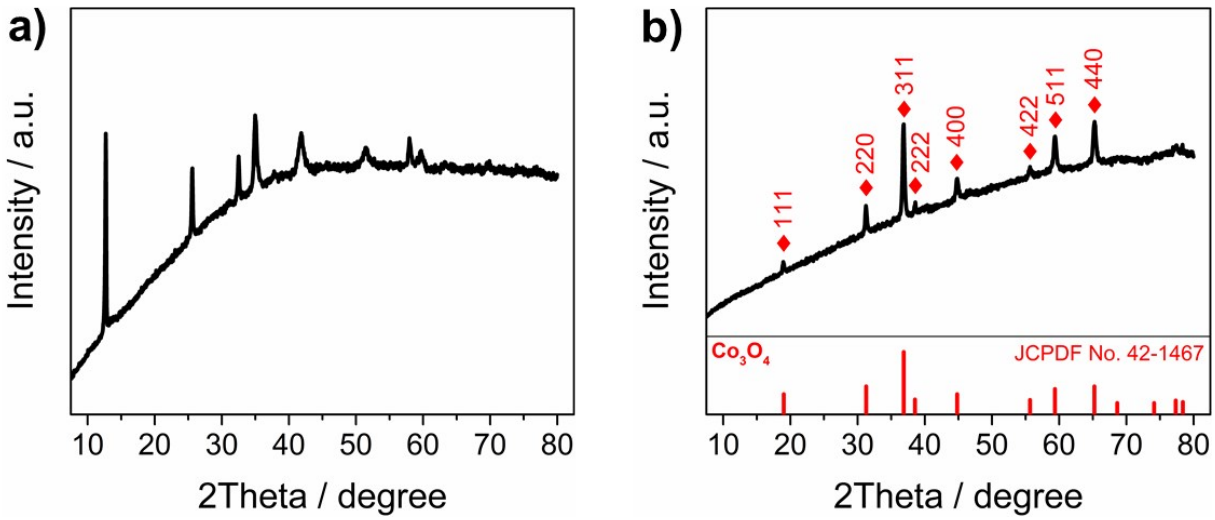

Figure S4. XRD patterns of (a) LCH nanosheets and (b) holey Co_3O_4 nanosheets. It can be seen that the XRD pattern of LCH is almost the same to those in previous works,[S3, S4] despite that their reflection intensities are different.

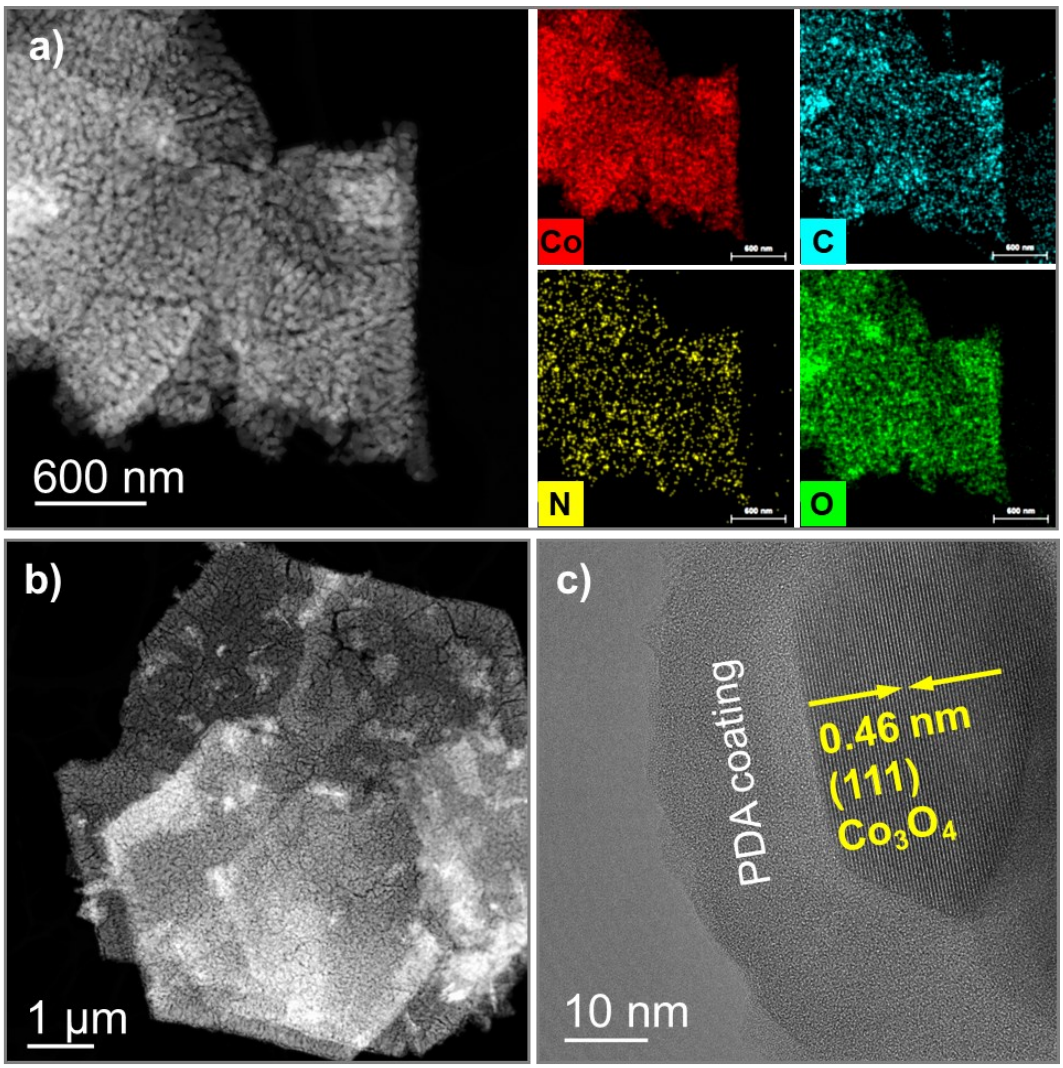

Figure S5. (a) STEM image with element mappings, and (b) STEM and (c) HRTEM images of the PDA coated holey Co_3O_4 nanosheets.

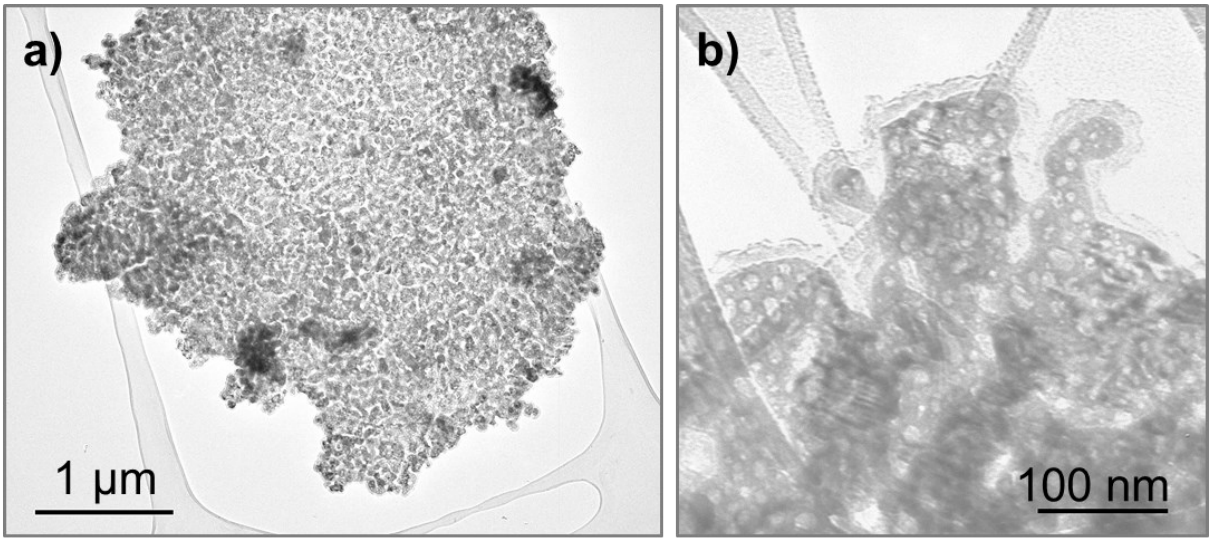

Figure S6. (a) Low-magnification and (b) high-magnification TEM images of the HPCO@NC nanohybrids. It can be seen that the pores exist inside the HPCO nanosheets rather than inside the NG coating.

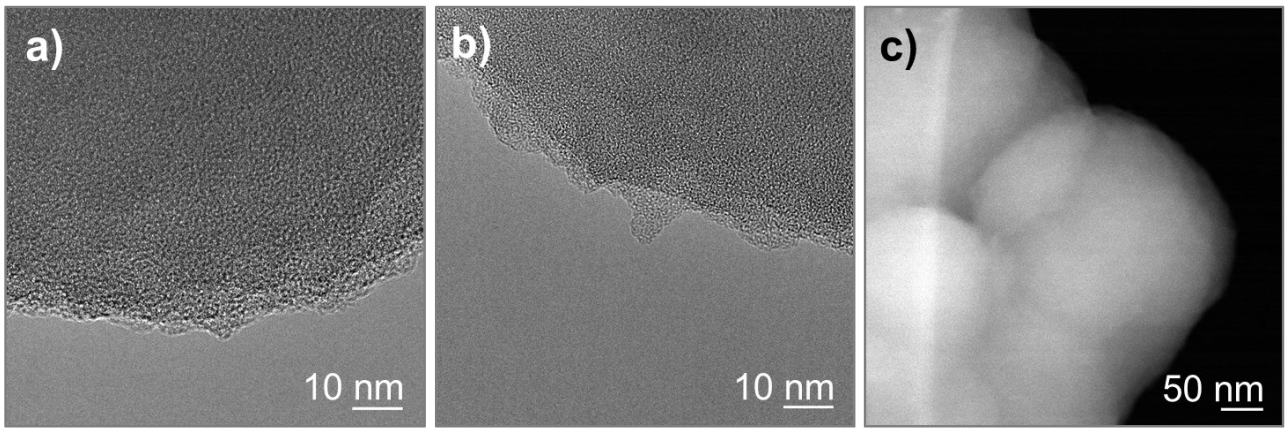

Figure S7. (a, b) TEM and (c) STEM images of NG that are obtained by the direct calcination of PDA in Ar atmosphere. There are no pores inside the NG, once more implying that the pores of HPCO@NG mainly exist in the HPCO nanosheets.

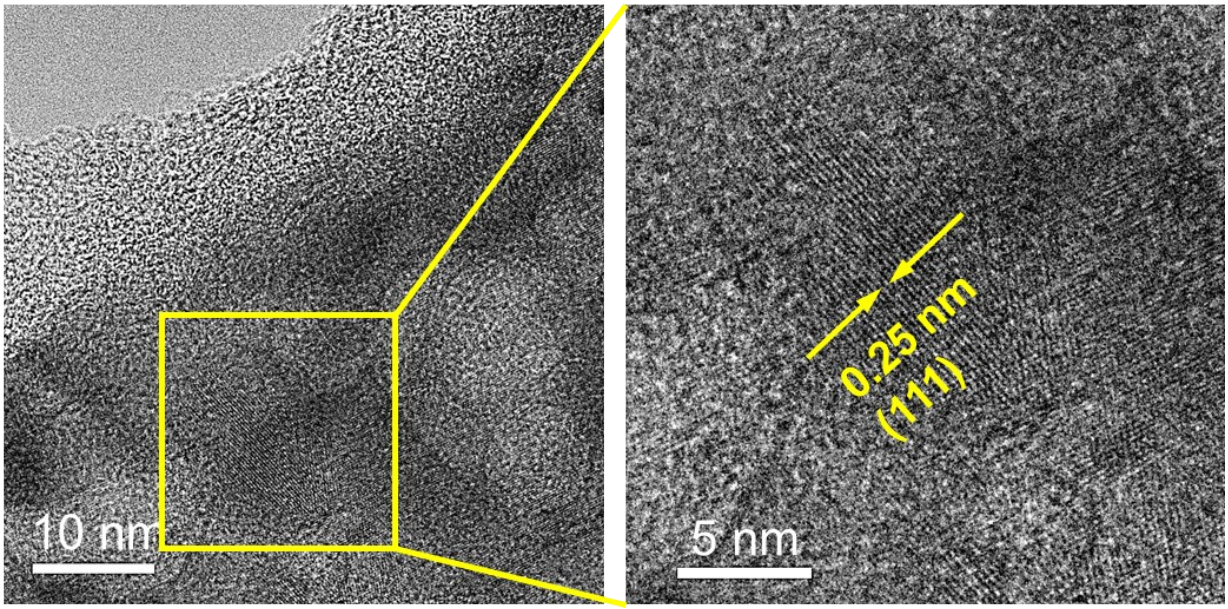

Figure S8. HRTEM images of the HPCO@NC nanohybrids.

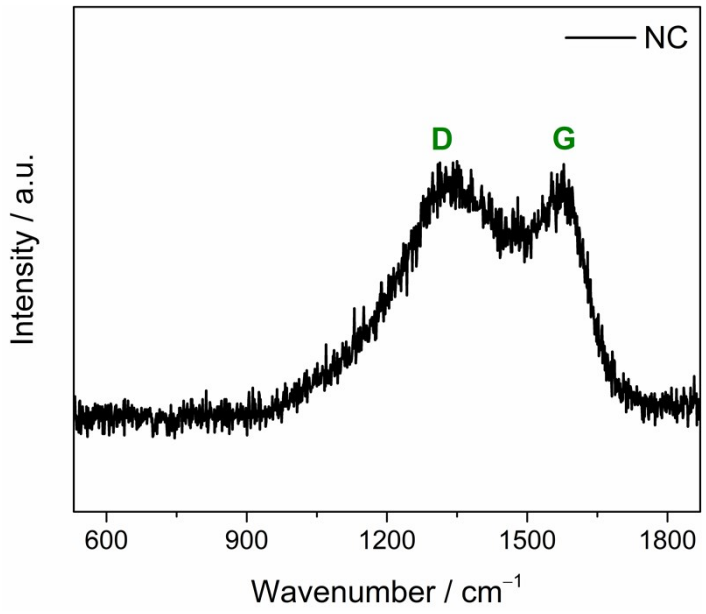

Figure S9. Raman spectrum of pure NG. The D band reflects the disordered structures of carbon network. The G band represents the characteristic peak of graphitic carbon. The noticeable D band implies that the NC is structurally disordered. [S5−S7]

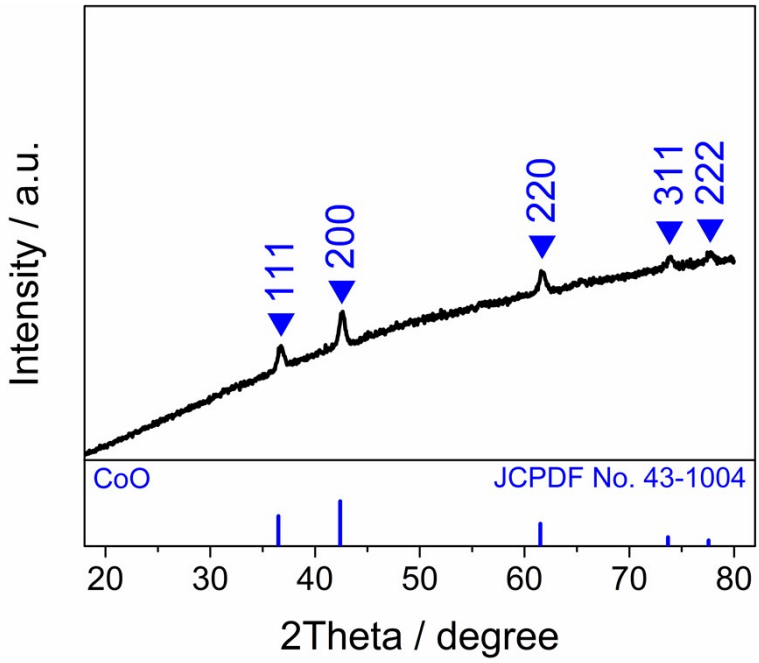

Figure S10. Raw XRD pattern of HPCO@NC.

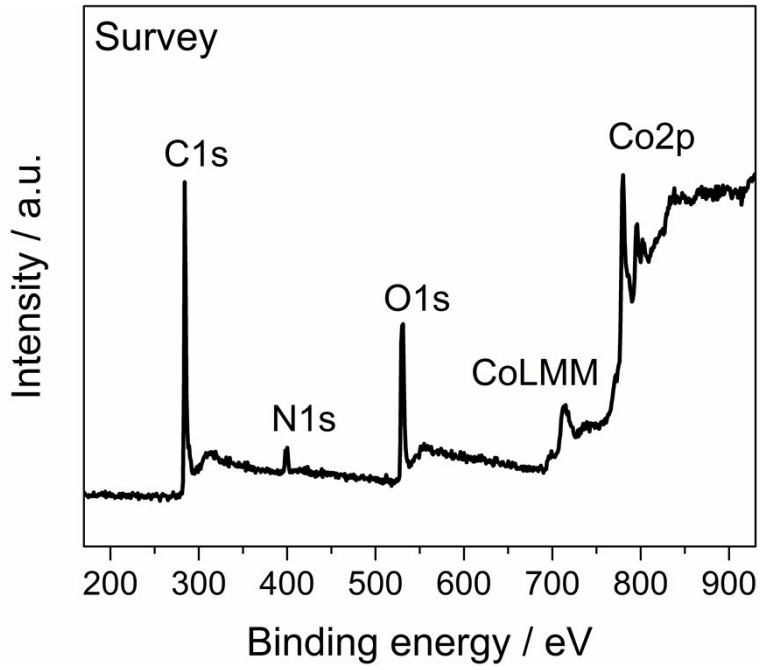

Figure S11. XPS survey spectrum of the HPCO@NC nanohybrids.

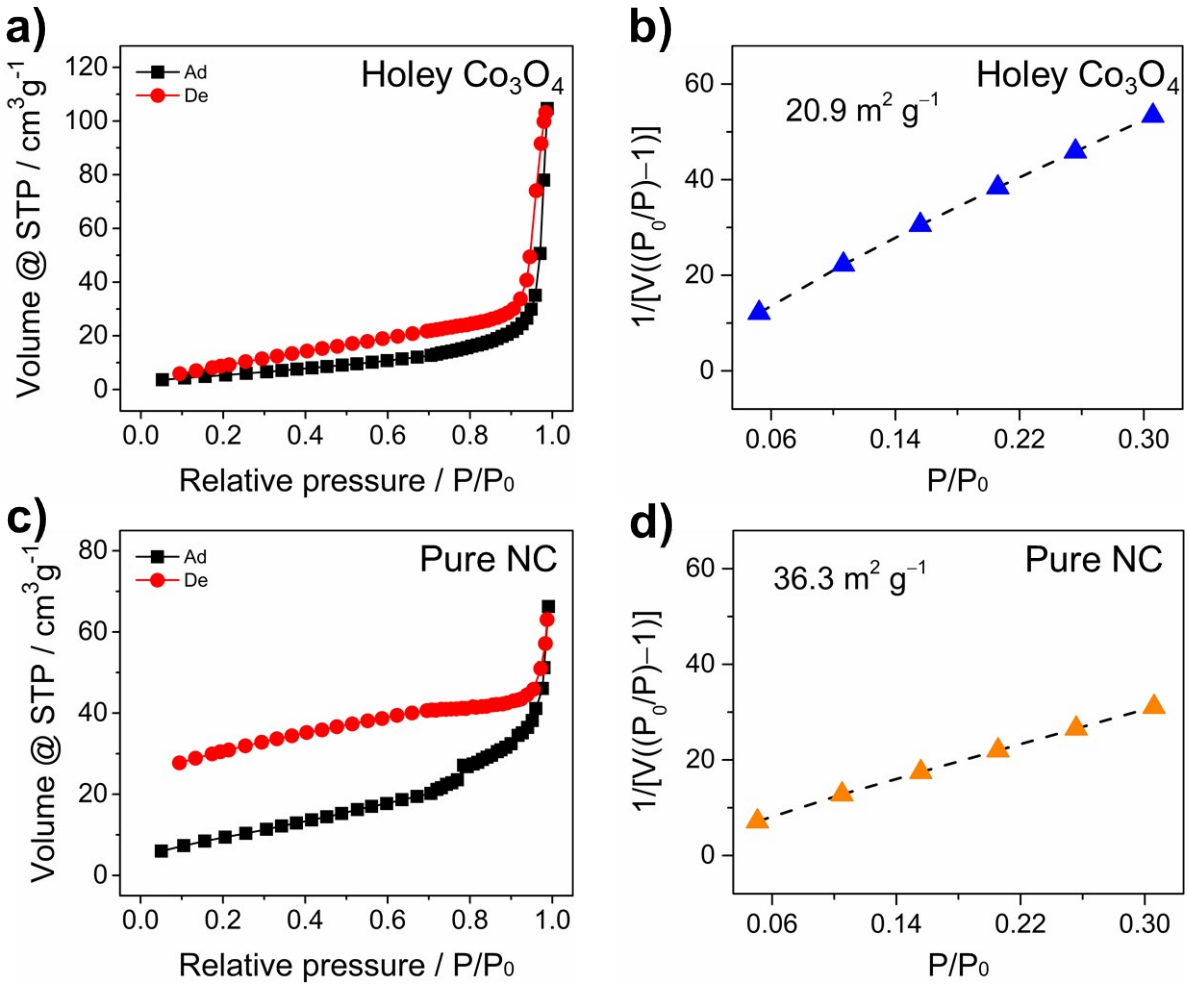

Figure S12. (a, c) N_2 adsorption-desorption isotherms and (b, d) BET curves of (a, b) holey Co_3O_4 nanosheets and (c, d) pure NC, respectively.

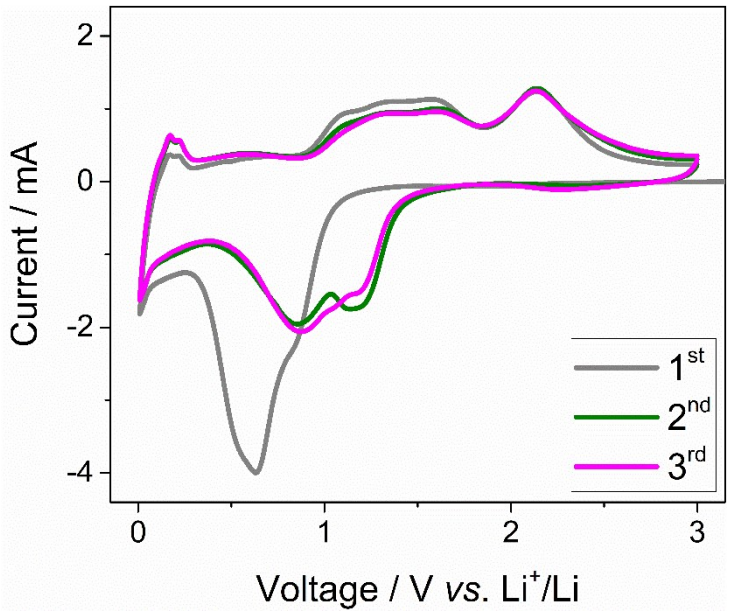

Figure S13. The first three CV curves of HPCO@NC nanohybrids at 0.1 mV s^{-1} (mass loading = 10 mg cm^{-2}).

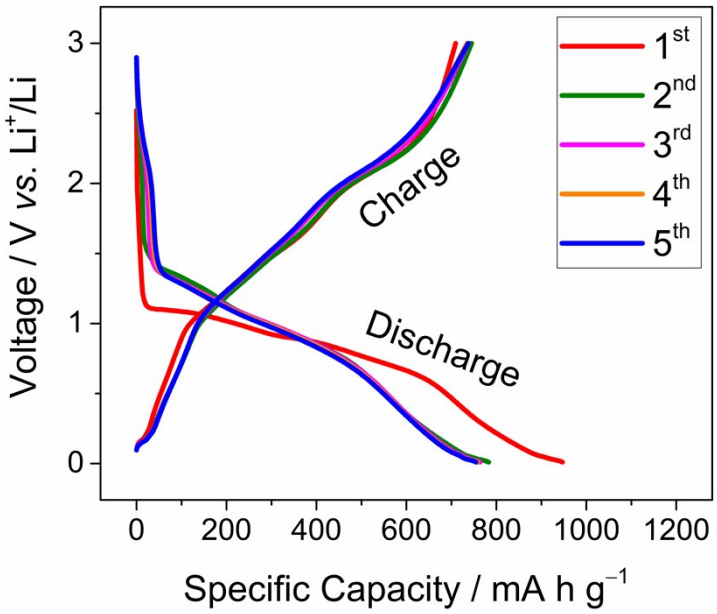

Figure S14. The first five discharge/charge profiles of HPCO@NC nanohybrids at 100 mA g^{-1} (mass loading = 10 mg cm^{-2}). The initial Coulombic efficiency is 74.9%, and it rises to 95.2% in the second cycle and further increases to 97.8% in the fifth cycle. These values are very close to those with a mass loading of 5 mg cm^{-2}, indicating the advantages of the holey porous structure for improving the Li^+ storage performance at high mass loadings.

Table S1. Comparison of areal capacities and rate capabilities of the HPCO@NC nanohybrids with other CoO/Co_3O_4-based anode materials

Materials & Structures	Mass Loading mg cm^{-2}	Cyclability			Rate Capabilities		Refs
		current density mA cm^{-2}	capacity mAh cm^{-2}	cycles	current density mA cm^{-2}	capacity mAh cm^{-2}	
CoP_3@carbon@CoO	2.5	1.25	2.88	80	0.25	3.56	[S8]
					0.5	3.48	
					1.25	3.06	
					2.5	2.57	
					5	2.10	
					12.5	1.43	
SnO_2-CoO@carbon	1.4	1.4	1.14	100	0.7	1.44	[S9]
		4.2	1.08	1000	1.4	1.22	
					2.8	1.08	
					7	0.89	
					14	0.71	
					21	0.59	
					28	0.45	
					35	0.43	
					42	0.37	
CoO@N,S-codoped carbon	0.8	0.08	1.32	100	0.08	1.30	[S10]
		0.8	0.65	500	0.24	1	
					0.72	0.80	
					0.96	0.71	
Co/CoO@carbon	1.0	0.5	0.62	500	0.2	0.79	[S11]
		1	0.58	2000	0.4	0.69	
		2	0.44	2000	1	0.57	
		5	0.3	10000	2	0.48	
					5	0.38	
					10	0.30	
					20	0.20	
Holey Co_3O_4	1.0	1	1	200	0.4	1.35	[S12]
					0.8	1.16	
					1.6	0.87	
					3.2	0.64	
					5	0.50	
Mesoporous Co_3O_4	–	0.74	4.39	30	0.74	4	[S13]
					1.85	3.74	
					3.69	2.99	
					7.38	1.61	

		0.16	0.91	100	0.08	0.81	
		0.82	0.49	750	0.16	0.80	
					0.41	0.77	
Co_3O_4/Graphene	0.82				0.82	0.74	[S14]
					1.64	0.67	
					4.10	0.56	
					8.20	0.29	
		0.25	1.40	100	0.06	1.47	
					0.13	1.56	
					0.25	1.51	
C-doped Co_3O_4	1.0~1.5*				0.6	1.32	[S15]
					1.25	1.16	
					2.5	0.94	
					3.75	0.76	
		1	7.14	50	1	7.55	
					2	6.82	**This work**
HPCO@NC	**10**				5	4.90	
					8	3.92	
					10	3.16	

* An average of 1.25 mg cm^{-2} was adapted when we calculated the areal current densities and capacities.

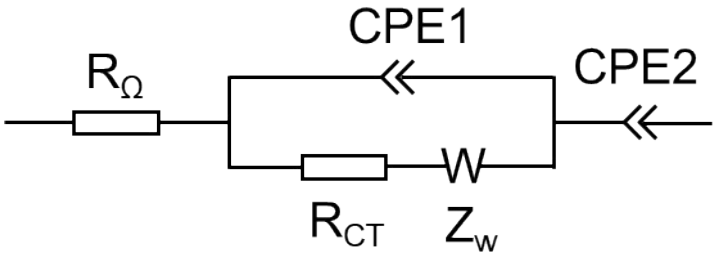

Figure S15. The equivalent circuit for Nyquist plots in **Figure 4i**.

Table S2. Fitted resistance of the HPCO@NC nanohybrids at different mass loadings.

Mass loading / mg cm^{-2}	R_Ω /Ω	R_{ct} / Ω
5	2.0	170.5
10	2.9	187.5

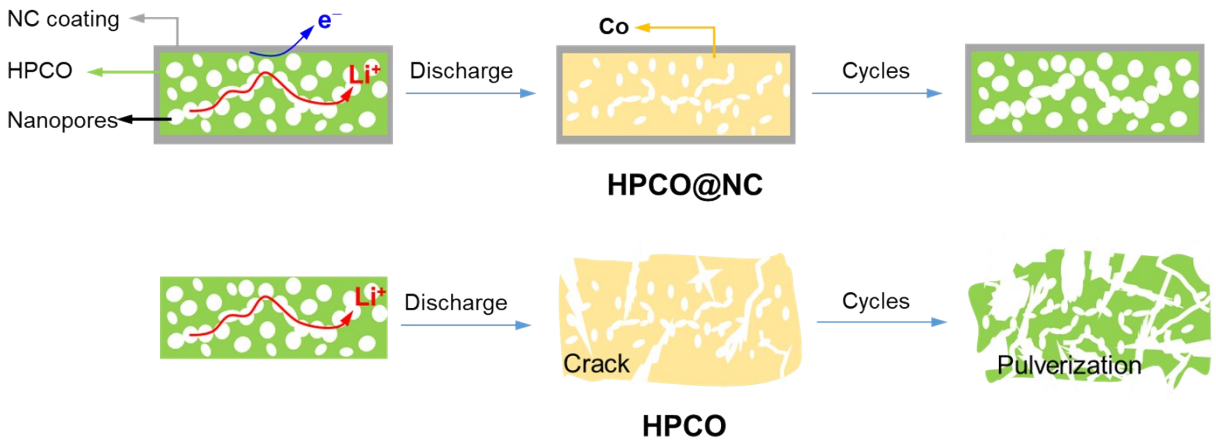

Figure S16. Sketch for the morphological and structural evolution of the HPCO@NC and HPCO upon cycling.

References

[S1] A. Małecki, J. A.K. Tareen, J. P. Doumerc, L. Rabardel, J. C. Launay, *J. Solid State Chem.*, **1985**, *56*, 49–57.

[S2] J. LÜ, C. Huang, S. Bai, Y. Jiang, Z. Li, *J. Nat. Gas Chem.*, **2012**, *21*, 37–42.

[S3] R. Xu, H. C. Zeng, *Chem*. *Mater*., **2003**, *15*, 2040−2048.

[S4] L. Pan, H. Huang, M. Niederberger, *J*. *Mater*. *Chem*. *A*, **2019**, *7*, 21264–21269.

[S5] F. Tuinstra, J. L. Koenig, *J*. *Chem*. *Phys*., 1970, 53, 1126–1130.

[S6] M. A. Pimenta, G. Dresselhaus, M. S. Dresselhaus, L. G. Cançado, A. Jorio, R. Saito, *Phys*. *Chem*. *Chem*. *Phys*., **2007**, *9*, 1276–1291.

[S7] L. Pan, H. Huang, M. Zhong, M. Niederberger, *Energy Storage Mater.*, **2019**, *16*, 519–526.

[S8] Y. Du, W. Ma, H. Li, *Small*, **2020**, *16*, 1907468.

[S9] J. H. Choi, G. D. Park, D. S. Jung, Y. C. Kang, *Chem*. *Eng*. *J*., **2019**, *369*, 726–735.

[S10] F. Wang, H.-Y. Zhuo, X. Han, W.-M. Chen, D. Sun, *J*. *Mater*. *Chem*. *A*, **2017**, *5*, 22964–22969.

[S11] X. Sun, G.-P. Hao, X. Lu, L. Xi, B. Liu, W. Si, C. Ma, Q. Liu, Q. Zhang, S. Kaskel, O. G. Schmidt, *J*. *Mater*. *Chem*. *A*, **2016**, *4*, 10166–10173.

[S12] D. Chen, L. Peng, Y. Yuan, Y. Zhu, Z. Fang, C. Yan, G. Chen, R. Shahbazian-Yassar, J. Lu, K. Amine, G. Yu, *Nano Lett*., **2017**, *17*, 3907−3913.

[S13] X. Wang, Y. Fan, R. A. Susantyoko, Q. Xiao, L. Sun, Deyan He, Q. Zhang, *Nano Energy*, **2014**, *5*, 91–96.

[S14] Y. Yang, J. Huang, J. Zeng, J. Xiong, J. Zhao, *ACS Appl. Mater. Interfaces*, **2017**, *9*, 32801−32811.

[S15] C. Yan , G. Chen, X. Zhou, J. Sun, C. Lv, *Adv*. *Funct*. *Mater*., **2016**, *26*, 1428–1436.